

Towards wafer scale inductive characterization of spin transfer torque critical current density of magnetic tunnel junction stacks

S. Sievers¹, N. Liebing¹, S. Serrano-Guisan², R. Ferreira², E. Paz², A. Caprile³, A. Manzin³, M. Pasquale³, W. Skowroński⁴, T. Stobiecki⁴, K. Rott⁵, G. Reiss⁵, J. Langer⁶, B. Ocker⁶, H.W. Schumacher¹

¹Physikalisch-Technische Bundesanstalt, Braunschweig, Germany (e-mail: sibylle.sievers@ptb.de)

²International Iberian Nanotechnology Laboratory, Braga, Portugal

³Istituto Nazionale di Ricerca Metrologica, Torino, Italy

⁴AGH University of Science and Technology, Department of Electronics, Krakow, Poland

⁵Bielefeld University, Department of Physics, Bielefeld, Germany

⁶Singulus Technologies, Kahl am Main, 63796, Germany

Abstract

We explore the prospects of wafer scale inductive probing of the critical current density j^{c0} for spin transfer torque switching of a CoFeB/MgO/CoFeB magnetic tunnel junction with varying MgO thickness. From inductive measurements magnetostatic parameters and the effective damping are derived and j^{c0} is calculated based on spin transfer torque equations. The inductive values compare well to the values derived from current induced switching measurements on individual nanopillars. Using a wafer scale inductive probe head could in the future enable *wafer probe station* based metrology of j^{c0} .

Terms—Critical current density, spin transfer torque, MRAM

I. INTRODUCTION

Spin transfer torque (STT) is the basis of promising applications like STT oscillators, and magnetic random access memories (MRAM) [1]. One of the key material parameters for STT applications is the critical current density j^{c0} . It determines the conditions at which, depending on the device application, STT induced precessional self oscillations set in or at which current

induced magnetization switching (CIMS) can be achieved. For MRAM applications this value is critical with respect to power consumption, drive circuit layout, storage density, write times, and the write/read threshold. It thus needs to be well optimized during material development and device design and tightly controlled during manufacturing. Today, determining j^{c0} of a STT material such as a magnetic tunnel junction (MTJ) stack is a time consuming process. First, individual nanopillars with electrical contacts are fabricated from the MTJ stack by a multi mask high resolution clean room lithography process. Then the pillars are electrically contacted and CIMS experiments are carried out to determine j^{c0} . Formerly, two other key MRAM material parameters, the tunnel magneto resistance (TMR) and the resistance area (RA) product could also only be determined on individually contacted devices. However, later a lithography-free testing scheme using current in-plane tunneling [2] enabled fast material research and wafer scale testing [3] thereby boosting MRAM and MTJ sensor development. In analogue, the development of a lithography-free and wafer scale characterization scheme for j^{c0} could underpin efficient STT material development and could allow fast wafer scale in-line testing for quality control.

Here we explore the prospects of wafer scale inductive probing of j^{c0} of a typical MRAM material: a CoFeB/ MgO/ CoFeB based MTJ stack with varying MgO thickness t_{MgO} . From ferromagnetic resonance (FMR) measurements [4] of the unpatterned MTJ stacks we derive the magnetostatic parameters and the effective damping α as function of t_{MgO} and calculate j^{c0} using the spin transfer torque equations [5]. The derived values of j^{c0} compare well to the values derived from current induced switching measurements on individual nanopillars of the same MTJ stack. We further compare the relevant parameters derived from inductive measurements using a standard coplanar waveguide [6] and using an inductive probe head suitable for wafer scale testing [7]. From the comparison we conclude that wafer scale inductive determination of j^{c0} of STT materials seems possible.

Ferromagnetic resonance (FMR) measurements of magnetic thin films and multilayers can be carried out using either cavity based or coplanar waveguide based systems. The latter can be carried out in time domain using pulsed inductive microwave magnetometry (PIMM) [8] or in frequency domain by vector network analyzer (VNA) FMR [9]. The coplanar broad band techniques deliver the FMR frequency f_{FMR} and the line with Δf as function of magnetic field. Fitting f_{FMR} to a Kittel model yields the magnetostatic material parameters (saturation magnetization M_S , anisotropy K_i , ...) and also interlayer exchange coupling J_{FL} between ferromagnetic layers. Analysis of Δf yields the effective magnetization damping α_{eff} . Note that according to Slonczewski's STT model j^{c0} is directly proportional to α_{eff} , M_S and the effective anisotropy of the material [10,11,12]. Hence, one can calculate j^{c0} based on the static and dynamic parameters derived from inductive measurements.

In the first part of this work we summarize the theory for the calculation of j^{c0} based on the inductive characterization of an MTJ sample. In the second part α_{eff} and M_S of a set of MTJ test structures with different MgO barrier thickness t_{MgO} are determined

from inductive measurements [4] and the corresponding critical current densities are calculated. The feasibility of the inductively derived j^{c0} is confirmed by CIMS data obtained on patterned nanopillars from the same material stack [13]. In the last part we compare the inductive measurements of a further MTJ stack using two different inductive setups: a standard coplanar wave guide and a recently developed wafer scale inductive probe head [7].

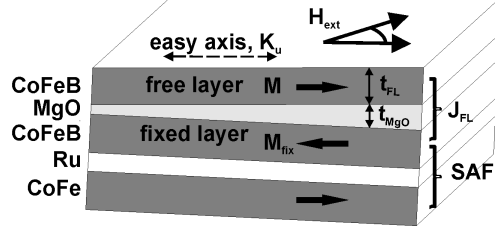


FIG. 1. Simplified sketch of the MTJ stack. The CoFe layer of the synthetic antiferromagnet (SAF) fixing the CoFeB layer is pinned to a PtMn antiferromagnet (not shown).

II. THEORY

In our experiments we study an MTJ, which is modeled as a coupled two layer system consisting of a free layer (FL) with in-plane magnetization \mathbf{M} , thickness t_{FL} and saturation magnetization M_S and a fixed layer as a reference layer with an in-plane magnetization \mathbf{M}_{fix} . The FL has an in-plane uniaxial anisotropy K_u and, at zero external field, the system has two stable magnetic states of the two electrodes, parallel (P) and antiparallel (AP). When currents are applied to the device, the magnetization dynamics of the FL can be described by the Landau-Lifshitz- Gilbert equation

$$\frac{d\mathbf{M}}{dt} = -\gamma\mu_0\mathbf{M} \times \mathbf{H}_{eff} - \frac{\alpha_{eff}}{M_S}\mathbf{M} \times \frac{d\mathbf{M}}{dt} + \tau_{STT} \frac{\mathbf{M} \times (\mathbf{M} \times \mathbf{M}_{fix})}{M_S^2 M_{fix}} + \tau_{FLT} \frac{\mathbf{M} \times \mathbf{M}_{fix}}{M_S M_{fix}}, \quad (1)$$

including the Slonczewski or in-plane STT term and the field-like or perpendicular STT term, respectively. Here, α_{eff} is the effective damping and γ the gyromagnetic ratio. According to this Slonczewski's model τ_{STT} is a function of the current density j , $\tau_{STT} = \gamma\hbar\eta/(2et_{FL})j$, e is the absolute value of the electronic charge and η is the spin-torque efficiency factor. The STT terms modify the magnetization dynamics of the device leading to magnetic excitations that can induce FL magnetization reversal. In zero external field the onset of such STT excitations is determined by τ_{STT} [14]:

$$\tau_{STT} = \alpha_{eff}\gamma M_S \left[\frac{2K_u}{M_S} + \frac{1}{2}\mu_0 M_S \pm \mu_0 H_{int} \right] = \alpha_{eff}\gamma M_S \mu_0 [H_u + H_D \pm H_{int}] = \alpha_{eff}\gamma M_S \mu_0 H_{eff}^0. \quad (2)$$

$H_{int} = J_{FL}/(t_{FL}\mu_0 M_S)$ is an interaction field taking into account both the magnetostatic and the exchange interaction J_{FL} between FL and fixed layer. $H_u = 2K_u/\mu_0 M_S$ is the uniaxial anisotropy field and $H_D = M_S/2$ is the demagnetizing field of the FL. They sum up to an effective field $H_{eff}^0 = H_u + H_D \pm H_{int}$.

For symmetric tunnel junctions this leads to a critical current expression for magnetization switching from P to AP $j_{P \rightarrow AP}^{c0}$ and AP to P $j_{AP \rightarrow P}^{c0}$

$$j_{P \rightarrow AP/AP \rightarrow P}^{c0} = \mp 2 \frac{e}{\hbar} \frac{\alpha_{eff} t_{FL} \mu_0 M_S}{\eta} H_{eff}^0, \quad (3)$$

with $\eta = 1/2 P/(1+P^2 \cos \Theta)$ [13,15]. The spin polarization P can be calculated from TMR values (using Julliere's model), which are accessible via non-destructive wafer scale measurements [3]. Thus, from the parameters α_{eff} , M_S , J_{FL} and K_u we can calculate j^{c0} .

A determination of these parameters is possible from non-invasive inductive techniques as will be discussed for the example of VNA-FMR measurements. The resonance frequency f_{FMR} is determined by the free energy density function F . In case of a uniaxial anisotropy F is given by

$$F = -\mu_0 M_S H_{ext} m(\varphi) h(\varphi) - \frac{\mu_0}{2} M_S^2 \cos^2(\theta) - K_u \sin(\theta) \cos^2(\phi) - \frac{J_{FL}}{t_{FL}} \cos(\phi), \quad (4)$$

where φ and ϕ are the azimuthal (in-plane) coordinates of the FL magnetization and the external field H_{ext} , respectively, with respect to M_{fix} , and θ is the polar (out-of-plane) coordinate of the FL magnetization. From F , following the ansatz of Smit and Beljers [16] the field dependence of the precession frequency can be derived:

$$f_{FMR} = \frac{\gamma \mu_0}{2\pi} \sqrt{H_{ext} \cos(\varphi - \phi) + H_u \cos(2\phi) + H_{int} \cos(\phi)} \cdot \sqrt{H_{ext} \cos(\varphi - \phi) + H_u \cos^2(\phi) + H_{int} \cos(\phi) + M_S}. \quad (5)$$

By fitting this model to the measured field dependence of f_{FMR} from the FMR measurements H_u , H_{int} and M_S can be found. Eq. 5 also holds for time domain (PIMM) measurements.

The last parameter inquired for the j^{c0} calculation is the effective damping α_{eff} . The effective damping emerges from the linewidth of the FMR peak. In case of small damping the imaginary part of the absorption peak can be fitted to a Lorentzian Function with the line width Δf :

$$\alpha_{eff} = \frac{4\pi}{\gamma \mu_0 M_S} \Delta f. \quad (6)$$

In summary from non invasive inductive measurements like PIMM or VNA-FMR we can deduce the intrinsic magnetic properties of the sample necessary to calculate j^{c0} .

III. EXPERIMENTS: INDUCTIVE DETERMINATION OF J^{c0}

For the comparison of CIMS and inductive measurements we studied MTJ stacks with different thicknesses of the tunneling barrier on Si wafers with a layer sequence: Ta(5)/CuN(50)/Ta(3)/CuN(50)/Ta(3)/PtMn(16)/CoFe(2)/Ru(0.9)/Co₄₀Fe₄₀B₂₀(2.3)/MgO(t_{MgO})/Co₄₀Fe₄₀B₂₀(2.3)/Ta(10)/CuN(30)/Ru(7) from bottom to top [17]. Numbers in parentheses refer to the layer thickness in nm. The MgO thickness is varied from $t_{\text{MgO}}=0.62$ to 0.96 nm without changing the remaining stack. The CoFe layer is the bottom part of a synthetic antiferromagnet (SAF) and is pinned by coupling to the antiferromagnetic PtMn.

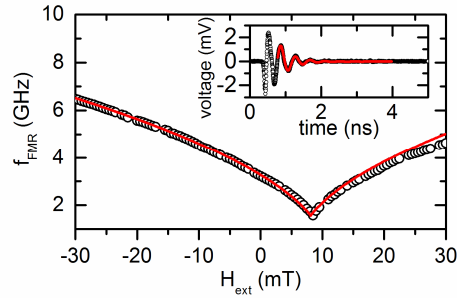


FIG. 2. Static field dependence of f_{FMR} derived from PIMM for $t_{\text{MgO}} = 0.76$ nm. Red line is the fit to Eq. (5). The inset shows the inductive PIMM data at 5mT easy axis field and the fit to a damped sinusoid (red).

CIMS measurements were performed on about five nanopillars for each $t_{\text{MgO}}=(0.96,0.88,0.82$ and $0.71)$ nm by applying voltage pulses of length $1 \text{ ms} \leq \tau \leq 54 \text{ ms}$. Details can be found elsewhere [13]. The J^{c0} from CIMS serve as reference to validate the inductive measurements. The TMR and RA were determined by wafer scale measurements using a commercial current in-plane tunneling setup [2,3]. For thick MgO barriers ($t_{\text{MgO}} \geq 0.75$ nm) the TMR ratio is high (TMR > 150%) and almost thickness independent. For thinner barriers ($t_{\text{MgO}} < 0.71$ nm) it drops significantly, pointing to possible barrier imperfections.

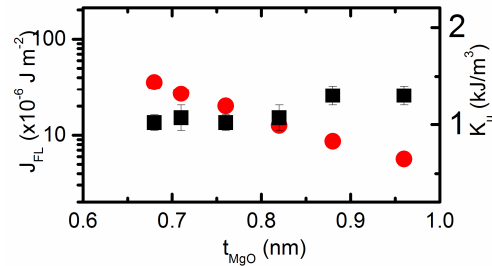


FIG. 3. (Color online) MgO thickness dependence of the coupling J_{FL} between free and reference layer (red circles) and uniaxial anisotropy energy K_u of the free layer (squares) from PIMM measurements.

For inductive characterization pieces of $2 \times 4 \text{ mm}^2$ lateral dimension were cut from the MTJ wafer. PIMM measurements were performed at room temperature with easy axis external field. The MTJ stacks were placed on top of a coplanar waveguide

(CPW) contacted with microwave probes. The setup can be used both for frequency domain and time domain inductive measurements. Details of this “standard” setup and the PIMM measurement technique are reported elsewhere [6,18]. From a single time resolved PIMM measurement at a given external field H_{ext} , the precession frequency and the damping parameter of the FL at this field value can be extracted by fitting to an exponentially damped sinusoid. The inset to Fig. 2 shows typical time resolved PIMM data for $t_{\text{MgO}}=0.76$ nm and $H_{\text{ext}}=-5$ mT. The measured field dependence of the FL precession frequency (open dots) was fitted by the model function in Eq. (5) (red line) to determine the FL magnetic parameters M_S , K_u and J_{FL} of the MTJ stacks. A constant magnetization saturation of $M_S=1.35$ T is obtained for all samples. The results for J_{FL} , K_u and α_{eff} are summarized in Figs. 3 and 4.

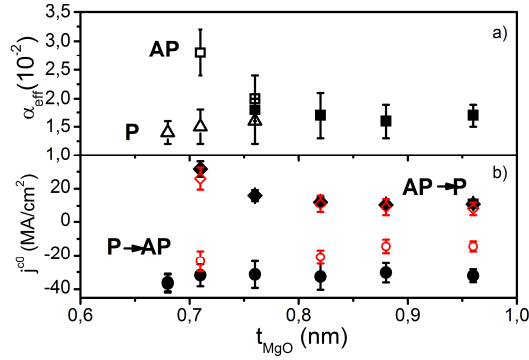


FIG. 4 (a): effective damping α_{eff} vs. MgO thickness. Open triangles refer to the damping parameter at parallel (α_{P}), open squares to the damping parameter at antiparallel configurations (α_{AP}). Full squares to equal α_{eff} of both configurations. b): Inductively determined j^{c0} (black symbols) for P \rightarrow AP ($j_{\text{P} \rightarrow \text{AP}}^{c0}$, circles) and AP \rightarrow P ($j_{\text{AP} \rightarrow \text{P}}^{c0}$, rhombs) switching. Red symbols show j^{c0} as determined from CIMS experiments on individual nanopillars.

In Fig. 3 J_{FL} shows an exponential decrease with the barrier thickness for $t_{\text{MgO}} \geq 0.7$ nm. At low thicknesses a ferromagnetic coupling between the FL and the fixed layer is observed. In contrast K_u shows no significant thickness dependence. In Fig. 4(a) three different regimes of α_{eff} can be observed, depending on t_{MgO} : for $t_{\text{MgO}} > 0.76$ nm no influence of the FL magnetization orientation (AP,P) on the FL damping is found and an almost constant value of $\alpha_{\text{eff}} \sim 0.017 \pm 0.01$ is observed. For $0.68 \text{ nm} < t_{\text{MgO}} < 0.76$ nm a different α_{eff} is obtained in the AP/P state ($\alpha_{\text{AP}}/\alpha_{\text{P}}$ marked by open squares/triangles). The measured increased damping in AP state is attributed to *orange-peel* coupling at low t_{MgO} due to barrier roughness [4]. At even lower barrier thickness FL precession is only observed in the P state and α_{AP} cannot be determined. Note that this thickness range below $t_{\text{MgO}}=0.7$ nm is not suitable for MRAM applications as no stable AP state can be realized. These inductively determined parameters are used to calculate the expected j^{c0} as a function of t_{MgO} as shown in Fig. 4 (b).

The black symbols mark the inductively determined values of j^{c0} for AP \rightarrow P (full rhombs) and P \rightarrow AP (full circles). In the case of unequal effective damping for P, AP the according relevant values α_P (P \rightarrow AP) or α_{AP} (AP \rightarrow P) were used to determine $j_{P\rightarrow AP}^{c0}$ and $j_{AP\rightarrow P}^{c0}$. The red open symbols mark the values of j^{c0} as determined from CIMS experiments on nanopillars fabricated from the same MTJ stack. For AP \rightarrow P switching both data sets show an excellent agreement over the whole range of t_{MgO} confirming the feasibility of inductive determination of j^{c0} . For P \rightarrow AP reversal a deviation of the two values beyond the measurement uncertainty is found for $t_{MgO} > 0.85$ nm. Here the inductively determined j^{c0} exceeds the CIMS value by about 50 %. The reason for the difference for AP \rightarrow P and P \rightarrow AP is not fully clear. It might be related to the influence of a field like torque or different resistive heating in the P and AP states during CIMS. Note, however, that for the lower thickness range of P \rightarrow AP reversal the inductive and CIMS data of j^{c0} agree within the measurement uncertainty. Note further that the general trends of the thickness dependence of j^{c0} of both data sets agree well. For $t_{MgO} > 0.75$ nm j^{c0} is almost independent of t_{MgO} . In contrast for lower t_{MgO} the absolute value of j^{c0} increases with decreasing t_{MgO} . Especially for AP \rightarrow P this increase can be well explained by the increase of α_{AP} due to orange peel coupling via the thin MgO barrier. To summarize, the results of the inductively determined j_{C0} show a good agreement with the CIPT measurements opening the path towards a future inductive and non-destructive determination of this key STT material parameter.

IV. INDUCTIVE PROBE HEAD MEASUREMENTS

We have previously described a CPW probe head (PH) suitable for wafer scale FMR [7]. The head consists of a CPW with rear contacts that can be brought in contact with the magnetic film on a wafer. So far it has been tested on single layer magnetic thin films. In the following we will compare FMR results of an MTJ stack using the wafer scale PH-FMR and our standard (S)-FMR as used in Sec. III.

We compare the inductive data obtained on a similar MTJ stack as described above, but with different thickness of the magnetic layers: Ta(5)/CuN(50)/ Ta(5)/CuN(50)/ Ta(5)/Ru(5)/ IrMn(20)/ CoFe(2)/ Ru(0.85)/ Co₄₀Fe₄₀B₂₀(2.6)/ MgO(t_{MgO})/ Co₄₀Fe₄₀B₂₀(2)/Ta(10)/Ru(7) [17]. This wafer was cut into pieces of (i) 20x20mm² (larger than the PH size) to test ‘‘wafer scale’’ measurements and (ii) 5x5 mm² size for characterization by S-VNA. VNA-FMR measurements were performed using both setups [18]. f_{FMR} and Δf of the frequency domain resonances peaks were calculated by fitting the sum of a symmetric and an antisymmetric Lorentzian to the respective data. α_{eff} was calculated from measured Δf via Eq. 6.

A typical measurement result of f_{FMR} (a) and α_{eff} (b) is shown in Fig. 5. The data is shown for negative applied fields $\mu_0 H$ and hence for AP configuration (full configuration of FL, fixed layer and bottom SAF layer is sketched). Note that our PH setup allows the application of higher fields and hence the wider PH data range. In the overlapping data range f_{FMR} obtained by S-FMR

(red) and PH-FMR (black) agree well. Fitting f_{FMR} to Eq. 5 yields a good agreement of magnetostatic parameters: PH-FMR: $\mu_0 M_S = 0.84 \pm 0.02$ T, $J_{\text{FL}} = 13 \pm 1$ $\mu\text{J}/\text{m}^2$; S-FMR: $\mu_0 M_S = 0.81 \pm 0.02$ T, $J_{\text{FL}} = 12 \pm 1$ $\mu\text{J}/\text{m}^2$) with K_u set to 1200 J/m^3 . Note that the present centimeter size PH in contact with the MTJ wafer reveals transmission discontinuities due to standing GHz waves inhibiting data analysis for certain frequencies (PH data gaps). When f_{FMR} approaches these gaps the PH-FMR resonance data are no longer described by a Lorentzian and therefore, Δf derived from PH-FMR and hence PH- α_{eff} are artificially enhanced. This effect can be seen in Fig. 5(b) where α_{eff} derived by both setups is plotted. The S-FMR damping (red) is almost constant over the given measurement range yielding an average effective damping of $\alpha_{\text{eff}} = 0.047 \pm 0.003$. The PH-FMR data shows a slightly lower damping in the center of the accessible data ranges and a strong increase of α_{eff} when f_{FMR} approaches frequency gaps. Averaging over the displayed data yields $\alpha_{\text{eff}} = 0.04 \pm 0.01$, a comparable value as for the S data but with larger uncertainty.

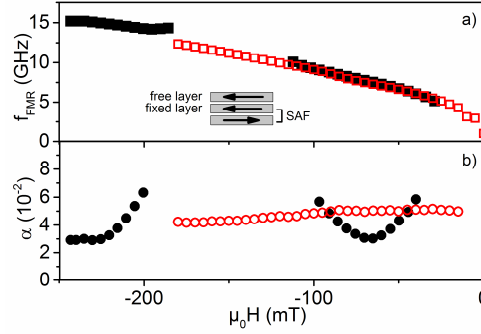


FIG. 5. (a) f_{FMR} vs. H measured by the inductive probe head (PH, black) and standard VNA-FMR (S, red open). Magnetic configuration is sketched. (b) α_{eff} as calculated from the linewidths of the resonance peaks from PH (black) and S (red open dots) measurements.

These results demonstrate the principal feasibility of a wafer scale FMR for the determination of key material parameters for STT MRAM. For future low uncertainty probing of j^{CO} the probe heads need further optimization to avoid detrimental CPW resonances. A possible approach might be a bended CPW on a flexible substrate with reduced contact area to the stack and a larger distance to the high frequency connectors.

This work was supported by EMRP JRP IND 08 MetMags. The EMRP is jointly funded by the EMRP participating countries within EURAMET and the European Union. W.S. and T.S. acknowledge Polish National Science Center statutory grant 11.11.230.016.

REFERENCES

- [1] See as a review e.g.: T. Kawaharaa, K. Itoa, R. Takemuraa, H. Ohnob, *Spin-transfer torque RAM technology: Review and prospect* Microelectronics Reliability **52**(4), 613–627 (2012).
- [2] D.C. Worledge and P. L. Trouilloud, Appl. Phys. Lett. **83**, 84 (2003).
- [3] CAPRES CIPTech; see www.capres.com.
- [4] S. Serrano-Guisan et al., *Inductive determination of the optimum tunnel barrier thickness in magnetic tunnelling junction stacks for spin torque memory applications*, J. Appl. Phys. **110**, 023906 (2011).
- [5] J. C. Slonczewski et al., *Theory of voltage-driven current and torque in magnetic tunnel junctions*, J. Magn. Magn. Mater. **310**, 169–175 (2007).
- [6] S. Serrano-Guisan et al., J. Phys. D: Appl. Phys. **41**, 164015 (2008).
- [7] S. Sievers, et al., *Towards Wafer Scale inductive Determination of Magnetostatic and Dynamic Parameters of Magnetic Thin Films and Multilayers*, IEEE Trans. Magn. **49**(1), 58, (2013).
- [8] T. J. Silva et al., *Inductive measurement of ultrafast magnetization dynamics in thin-film permalloy*, J. Appl. Phys., **85**(11), 7849, (1999).
- [9] S. V. Vonsovskii, *Ferromagnetic Resonance*, Pergamon Press, Oxford, 1966.
- [10] J. Z. Sun. *Spin-current interaction with a monodomain magnetic body: A model study*. Phys. Rev. B, **62**, 570 (2000).
- [11] H. Kubota et al., *Dependence of spin-transfer switching current on free layer thickness in CoFeB/MgO/CoFeB magnetic tunnel junctions*. Appl. Phys. Lett. **89**, 032505 (2006).
- [12] J. Hayakawa et al., *Current-induced magnetization switching in MgO barrier based magnetic tunnel junction with CoFeB/Ru/CoFeB synthetic ferromagnetic free layer*. Jpn. J. Appl. Phys. **45**, L1057 (2006).
- [13] W. Skowronski et al., *Interlayer exchange coupling and current induced magnetization switching in magnetic tunnel junctions with MgO wedge barrier*, J. Appl. Phys. **107**, 093917 (2010).
- [14] N.A. Pertsev, *Origin of easy axis magnetization switching in magnetic tunnel junctions with voltage-controlled interfacial anisotropy*, Sci. Rep. **3**, 2757 (2013).
- [15] L. Finocchio, G. and Azzerboni, B. and Fuchs, G. D. and Buhrman, R. A. and Torres, *Micromagnetic modeling of magnetization switching driven by spin-polarized current in magnetic tunnel junction*, , J. Appl. Phys. **101**, 063914 (2007).
- [16] J. Smit and H. G. Beljers, Philips Res. Rep. **10**, 113 (1955).
- [17] Samples are sputter deposited in a Singulus NDT Timaris Cluster Tool.

- [18] S. Serrano-Guisan, *Thickness dependence of the effective damping in epitaxial Fe_3O_4 /MgO thin films*, J. Appl. Phys. **109**, 013907 (2011).